PAPER

Check for updates

Substrate scope driven optimization of an encapsulated hydroformylation catalyst†

Pim R. Linnebank,[a] Alexander M. Kluwer[b] and Joost N. H. Reek [iD] *[ab]

Caged complexes can provide impressive selective catalysts. Due to the complex shapes of such caged catalysts, however, the level of selectivity control of a single substrate cannot be extrapolated to other substrates. Herein, the substrate scope using 41 terminal alkene substrates is investigated in the hydroformylation reaction with an encapsulated rhodium catalyst [Rh(H)(CO)$_3$(P($_m$Py$_3$(ZnTPP)$_3$))] (**CAT1**). For all substrates, the amount of branched products formed was higher with **CAT1** than with the unencapsulated reference catalyst [Rh(H)(CO)$_2$(P($_m$Py$_3$))$_2$] (**CAT2**) (linear/branched ratio between 2.14 and 0.12 for **CAT1** and linear/branched ratio between 6.22 and 0.59 for **CAT2**). Interestingly, the level of cage induced selectivity depends strongly on the substrate structure that is converted. Analysis of the substrate scope combined with DFT calculations suggests that noncovalent interactions between the substrate moieties and cage walls play a key role in controlling the regioselectivity. Consequently, these supramolecular interactions were further optimized by replacing the ZnTPP building block with a zinc porphyrin analog that contained OiPr substituents on the *meta* position of the aryl rings. The resulting caged catalyst, **CAT4**, converted substrates with even higher branched selectivity.

Introduction

Catalysts encapsulated in supramolecular architectures offer unique levels of selectivity that are mostly unattainable for traditional transition metal catalysts.[1–10] By encapsulating a transition metal within a cage, a microenvironment is created around the active catalyst, similar to enzymes. This microenvironment enables differentiation of reactive sites on the substrate that would otherwise be indistinguishable for a traditional transition metal catalyst. Encapsulated catalysts demonstrated impressive control over the site selectivity, regioselectivity, enantioselectivity and chemoselectivity for challenging substrates for several reactions such as the hydroformylation reaction,[11–20] allylic alkylation,[21] substrate selective isomerization reactions,[22] C–H activation,[23] site selective semihydrogenation reactions,[24] cyclopropanation,[25,26] epoxidation,[27–29] hydroboration[30] and gold-catalyzed cyclization reactions.[31–33]

A common and effective method for encapsulating transition metals is the ligand-template approach.[34,35] In this approach, the ligand has a dual role as it coordinates to the catalytically active metal while it also functions as a template for the self-assembly of the capsule. One of the pioneering examples in this regard is the application of [Rh(H)(CO)$_3$(P$_m$-Py$_3$(ZnTPP)$_3$)] (**CAT1**) as a caged hydroformylation catalyst (Fig. 1).[14,15] **CAT1** is formed by self-assembly by combining tris(*meta*-pyridyl)phosphine [P($_m$Py$_3$)] and three zinc *meso*-tetraphenylporphyrin (ZnTPP) units relying on the selective N–Zn coordination.[35] The phosphine atom coordinates to rhodium when reacted with [Rh(acac)(CO)$_2$)], and when using syngas (H$_2$:CO), the encapsulated hydroformylation catalyst **CAT1** is formed as depicted in Fig. 1.[35,36]

In a hydroformylation reaction, an alkene reacts with syngas (a mixture of H$_2$ and CO) in the presence of a transition metal catalyst to form an aldehyde. For terminal alkenes, often two different regioisomeric products are formed, the linear (l) and the branched (b) aldehyde (Fig. 2).[37–40] The application of **CAT1**
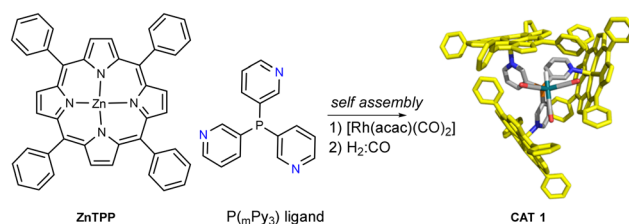
[a] *Homogeneous, Supramolecular and Bio-Inspired Catalysis, Van't Hoff Institute for Molecular Sciences University of Amsterdam, Science Park 904, 1098 XH Amsterdam, The Netherlands. E-mail: j.n.h.reek@uva.nl*
[b] *InCatT B.V, Science Park 904, 1098 XH Amsterdam, The Netherlands*
† Electronic supplementary information (ESI) available. See DOI: https://doi.org/10.1039/d4cy00051j

Fig. 1 The ligand-template approach for the formation of [Rh(H)(CO)$_3$(P($_m$Py$_3$(ZnTPP)$_3$))] (**CAT1**) (DFT modeled structure). ZnTPP building blocks are depicted in yellow for clarity.

This journal is © The Royal Society of Chemistry 2024

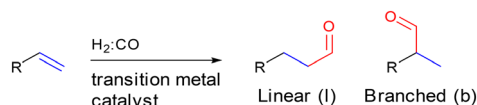*Catal. Sci. Technol.*, 2024, **14**, 1837–1847 | **1837**

Fig. 2 General scheme of the hydroformylation reaction showing that two regioisomers of the aldehyde product can be formed.

in the hydroformylation of aliphatic terminal alkenes leads to enhanced regioselectivity to form predominantly the branched aldehyde, which is due to the confinement of the alkene substrate (Fig. 3a). In analogy, the hydroformylation of internal alkenes leads dominantly to the product with the aldehyde on the innermost carbon atom (Fig. 3b and c) (Fig. 4).[14–17]

Branched product selectivity for terminal aliphatic alkenes, without isomerization as a side reaction, is remarkable as most catalysts convert such substrates with an excess to the linear aldehyde.[37,41,42] Only recently, three other catalysts have been reported that also convert aliphatic alkenes to form dominantly the branched product *i.e.* rhodium catalysts based on BOBPhos and TriPhos ligands.[43–47] There are some catalysts that produce the branched aldehyde, even in very high selectivity, but these also show a lot of isomerization, typically leading to a mixture of branched aldehyde products.[48–50] These catalysts can be very valuable in the hydroformylation of propene, as isomerization doesn't lead to other products.

The selectivity control of unfunctionalized internal alkenes by **CAT1** is even more remarkable as the alkene carbon atoms of internal alkene substrates are indistinguishable in terms of electronics and sterics for traditional hydroformylation catalysts.[16] These substrates do not contain a (supramolecular) directing group for differentiation between the two alkene carbon atoms[51–60] and this demonstrates the power of encapsulated catalysts to control the regioselectivity.
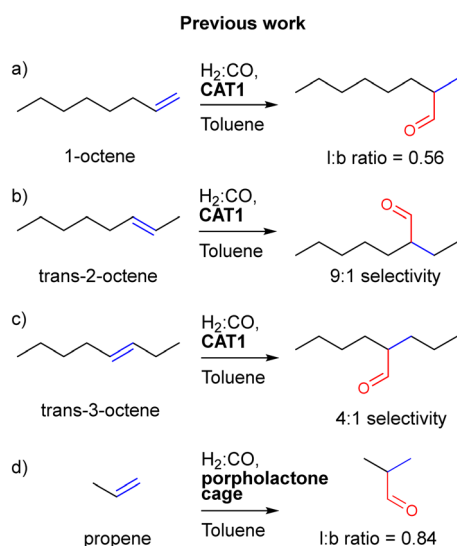

Fig. 3 Previously reported substrate scope of aliphatic alkenes using **CAT1** for the conversion of a) 1-octene, b) trans-2-octene, c) trans-3-octene, d) propene.
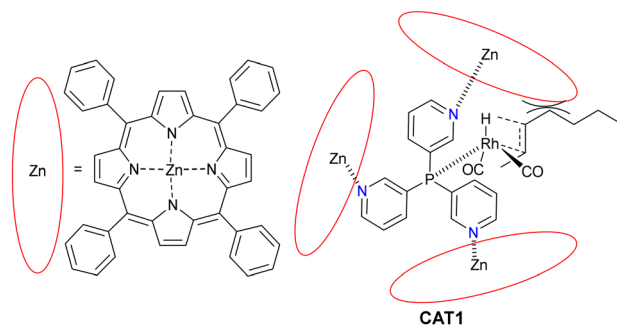

Fig. 4 The substrate rotation is blocked by the ZnTPP capsule for most of the catalytic pathways that lead to the outermost aldehyde.

Further improvements on **CAT1** have been made by employing an analog of ZnTPP, a porpholactone, that displays a stronger zinc–pyridine interaction than ZnTPP while forming an encapsulated rhodium catalyst similar to **CAT1**.[19]

Moreover, as the space around the metal center is slightly smaller, this cage can convert propene to mainly the branched product (l/b = 0.84) (Fig. 3d), where the branched product has significant industrial potential.[46,61] Recently, Dydio *et al.* reported a palladium based catalyst that was able to achieve exceptionally high branched selectivity for propene.[61] Experiments with other substrates showed significant isomerization, making this catalyst unsuitable for branched selective reactions of other alkyl alkenes.

To date, **CAT1** has only been investigated for linear terminal aliphatic alkenes such as 1-octene, 1-hexene and propene. Other terminal aliphatic alkenes of type R–CH₂– C=C have not been explored and we were interested to what extent the substrate structure would affect the regioselectivity control of **CAT1**. Herein, we report the evaluation of the substrate scope of terminal alkenes using both **CAT1** and a nonencapsulated analogue as a reference catalyst, **CAT2** (Fig. 5).[62] In a preliminary study, we have recently used part of the experimental data set to explore descriptor based approaches to understand the regioselectivity of these systems.[63]

Results and discussion

CAT1 has previously been studied in detail for the hydroformylation of 1-octene.[16] The binding constant of the first porphyrin to the tris(*meta*-pyridyl)phosphine was found
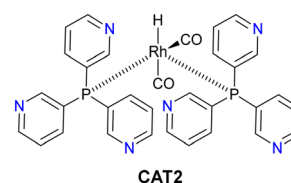

Fig. 5 Non-encapsulated reference catalyst [Rh(H)(CO)₂(P(ₘPy₃))₂] **CAT2** generated by combining [P(ₘPy₃)] and [Rh(acac)(CO)₂] under syngas conditions.

to be $K_1 = 2.5 \times 10^3$ M^{-1}, while the second and third porphyrin displayed a higher binding constant. This cooperative binding was explained by pi–pi interactions between adjacent porphyrins, as also confirmed by the X-ray structure. This high affinity ensures that under catalytic conditions, the structure is intact. Indeed, control experiments with an excess of ZnTPP show similar selectivity to those with the 3:1 ratio (ZnTPP/ P(mPy$_3$)), whereas at a lower ratio the selectivity is lost.[14,15,17,19] Compared to **CAT2**, the rhodium complex in **CAT1** is encapsulated, and at the same time the coordination around rhodium has changed from bisphosphorus to monophosphorus. It is well documented that this change in a coordination mode has an impact on both the activity and the selectivity. To distinguish between these effects, detailed theoretical studies have been carried out that concluded that the difference in catalyst performance is based on a combination of both.[15,64] For the remainder of the manuscript, we will refer to the encapsulation effect, which is a combination of the cage effect and change in coordination geometry.[62]

For the investigation of the current substrate scope, we evaluated 41 commercially available substrates using **CAT1** as the encapsulated catalyst and **CAT2** as the reference catalyst that is formed under the same conditions in the absence of ZnTPP. For this study, all reactions were conducted in toluene, at room temperature using 20 bar of syngas, identical to previously reported studies with **CAT1** as under these conditions, both catalysts display the same kinetic behavior. Apart from the presence of ZnTPP, all conditions were the same for each catalytic entry and every reaction was run for 48 h.

Since the different alkenes investigated in this study exhibit different biases towards the formation of one of the regioisomers, comparing the absolute linear/branched ratio is less meaningful. To obtain an estimate how effective **CAT1** is at enhancing branched product formation, we calculated the relative reaction barriers ($\Delta\Delta E$) based on the linear/branched ratio for every substrate obtained when **CAT1** or **CAT2** was applied as a catalyst. For these calculations, the Boltzmann distribution was used with k_B being the Boltzmann constant and T being the temperature in Kelvin at which the reaction was carried out:

$$\Delta\Delta E = \ln\left(\frac{\text{linear}}{\text{branched}}\text{ratio}\right) \times k_B T \times N_A \qquad (1)$$

With these energy values, we subtracted the $\Delta\Delta E$ obtained for **CAT1** from the $\Delta\Delta E$ displayed by **CAT2** for every substrate investigated:
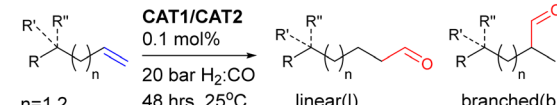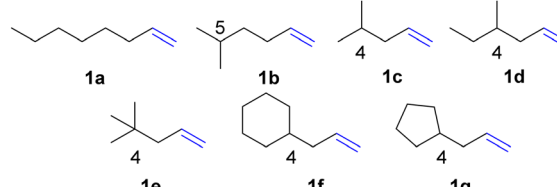
$$\text{Encapsulation effect} = \Delta\Delta E\ \textbf{CAT2} - \Delta E\ \textbf{CAT1} \qquad (2)$$

This energy difference was coined the "encapsulation effect" and reflects both the cage effect as a result of the formation of a capsule around rhodium and the change in coordination around rhodium.[14,15,65–67]

Aliphatic alkenes with remote substituents

First, we reacted the previously reported 1-octene and other aliphatic alkenes with substitution patterns on positions 4' and 5' and these catalytic results are presented in Table 1. **CAT1** gives full conversion after 48 h for these aliphatic substrates (**1a–1g**). In contrast, **CAT2** gives lower conversion, which is in line with the higher activity of the caged catalyst compared to the non-encapsulated analogue.[14,64] The selectivity obtained for 1-octene using **CAT1** matches the previously reported regioselectivity (l/b is 0.56), whereas the uncaged catalyst **CAT2** provides the aldehydes with an excess of the linear product. The regioselectivity obtained for 5-methylhexene **1b** is almost equal to that for 1-octene **1a** and thus this methyl group has no effect on the regioselectivity. For the substrates with a substituent on position 4, **1c–1g**, the branched selectivity was significantly higher with **CAT1** compared to 1-octene **1a** with the l/b ranging between 0.44 and 0.27. In particular, the substrates that have a five or six membered ring on position 4, i.e. allylcyclohexane **1f** and allylcyclopentane **1g**, are converted with high branched selectivity with **CAT1**. For the substrates

Table 1 Sub-class of aliphatic alkene substrates studied. Conditions: [Rh(acac)(CO)$_2$] = 0.70 mmol L^{-1} in toluene, pressure (H$_2$:CO) = 20 bar, substrate/rhodium = 1000, [P(mPy$_3$)] = 6.4 mmol L^{-1} and 19.2 mmol l^{-1} of zinc(II) tetraphenylporphyrin for **CAT1**. No significant isomerization and isomerization–hydroformylation products were observed for all entries

Substrate/catalyst	% conv[a]	l:b[b]	Encapsulation effect[c]
1a/CAT1	100	0.56	0.97 kcal mol^{-1}
1a/CAT2	70	2.88	
1b/CAT1	100	0.54	1.01 kcal mol^{-1}
1b/CAT2	75	3.04	
1c/CAT1	100	0.44	0.99 kcal mol^{-1}
1c/CAT2	44	2.46	
1d/CAT1	100	0.42	1.06 kcal mol^{-1}
1d/CAT2	41	2.51	
1e/CAT1	100	0.44	0.74 kcal mol^{-1}
1e/CAT2	46	1.52	
1f/CAT1	100	0.27	1.40 kcal mol^{-1}
1f/CAT2	96	2.86	
1g/CAT1	100	0.39	1.11 kcal mol^{-1}
1g/CAT2	84	2.55	

[a] Conversion determined by ^{1}H NMR spectroscopy. [b] The linear: branched ratio determined by GC. [c] The encapsulation effect calculated by subtracting the relative energy barriers of the encapsulated reaction outcome (using **CAT1**) from the unencapsulated reaction outcome (using **CAT2**).

1b–d, the encapsulation effect is similar to the parent **1a** substrate (an encapsulation effect of 0.97–1.06 kcal mol^{-1}). For 4,4′-dimethylpen-1-tene **1e**, the encapsulation effect is lower than the 1-octene **1a** encapsulation effect (0.73 kcal mol^{-1} for **1e** vs. 0.97 kcal mol^{-1} for **1a**), which shows that the higher branched selectivity of **1e** compared to **1a** is mostly caused by the electronic bias of the substrate.

Aliphatic alkenes with substituents close to the alkene

The second set of substrates for the scope evaluation focused on compounds that contain an additional alkyl substituent on position 3 (Table 2). These substrates display a wide variation of selectivity control with **CAT1** (l/b between 0.49 and 2.11). In contrast, the non-encapsulated catalyst **CAT2** converts all these substrates with a comparable regioselectivity (l/b of around 5.5), which is common for aliphatic alkenes bearing a substituent on position 3.[68,69] Interestingly, the encapsulation effect on **2a** and **2b** is higher than that observed for the parent substrate **1a**, showing that the presence of 5- and 6-membered rings close to the alkene increases the encapsulation effect and results in higher selectivity control. In contrast, when the ring size increases further, as is the case for **2d**, the regioselectivity control is lower.

Aliphatic alkenes with oxygen atoms in the chain

We next evaluated how the caged catalyst controls the regioselectivity of aliphatic alkenes that contain an ether (**3a–e**), ester (**3f–g**) or ketone (**3h**) substituent (Table 3).

Table 2 Sub-class of aliphatic alkene substrates with substituents close to the alkene. Conditions: [Rh(acac)(CO)$_2$] = 0.70 mmol L^{-1} in toluene, pressure (H$_2$:CO) = 20 bar, substrate/rhodium = 1000, [P($_m$Py$_3$)] = 6.4 mmol L^{-1} and 19.2 mmol l^{-1} of zinc(II) tetraphenylporphyrin for **CAT1**. No significant isomerization and isomerization–hydroformylation products were observed for all entries

Substrate/catalyst	% conv^a	l : b^b	Encapsulation effect^c
2a/CAT1	100	0.49	1.33 kcal mol^{-1}
2a/CAT2	80	4.62	
2b/CAT1	100	0.83	1.19 kcal mol^{-1}
2b/CAT2	53	6.22	
2c/CAT1	100	1.33	0.88 kcal mol^{-1}
2c/CAT2	73	5.91	
2d/CAT1	100	2.11	0.59 kcal mol^{-1}
2d/CAT2	69	5.75	

^{a} Conversion determined by ^{1}H NMR spectroscopy. ^{b} The linear : branched ratio determined by GC. ^{c} The encapsulation effect calculated by subtracting the relative energy barriers of the encapsulated reaction outcome (using **CAT1**) from the unencapsulated reaction outcome (using **CAT2**).

Table 3 Subset of aliphatic alkenes with oxygen atoms in the chain. Conditions: [Rh(acac)(CO)$_2$] = 0.70 mmol L^{-1} in toluene, pressure (H$_2$:CO) = 20 bar, substrate/rhodium = 1000, [P($_m$Py$_3$)] = 6.4 mmol L^{-1} and 19.2 mmol l^{-1} of zinc(II) tetraphenylporphyrin for **CAT1**. No significant isomerization and/or isomerization–hydroformylation products were observed for all entries

Substrate/catalyst	% conv^a	l:b^b	Encapsulation effect^c
3a/CAT1	89	0.59	0.49 kcal mol^{-1}
3a/CAT2	22	1.34	
3b/CAT1	100	0.57	0.50 kcal mol^{-1}
3b/CAT2	64	1.27	
3c/CAT1	100	0.32	0.36 kcal mol^{-1}
3c/CAT2	57	0.59	
3d/CAT1	82	0.55	0.24 kcal mol^{-1}
3d/CAT2	78	0.82	
3e/CAT1	100	0.34	1.20 kcal mol^{-1}
3e/CAT2	30	2.60	
3f/CAT1	100	0.21	1.07 kcal mol^{-1}
3f/CAT2	98	1.27	
3g/CAT1	100	0.47	0.90 kcal mol^{-1}
3g/CAT2	84	2.14	
3h/CAT1	100	0.50	0.95 kcal mol^{-1}
3h/CAT2	84	2.50	

^{a} Conversion determined by ^{1}H NMR spectroscopy. ^{b} The linear : branched ratio determined by GC. ^{c} The encapsulation effect calculated by subtracting the relative energy barriers of the encapsulated reaction outcome (using **CAT1**) from the unencapsulated reaction outcome (using **CAT2**).

For the allylether type substrates **3a–d**, there is only a minor difference between the regioselectivity displayed by the encapsulated catalyst **CAT1** and the unencapsulated catalyst **CAT2**, albeit that **CAT1** converts these substrates with higher branched selectivity than **CAT2**. This is also reflected in the low encapsulation effects ranging between 0.24 kcal mol^{-1} and 0.50 kcal mol^{-1}. For these substrates, the branched selectivity is already high for **CAT2** due to the polarization of the C=C bond.[70,71] In contrast, 4-methoxybut-1-ene (**3e**), a substrate in which the ether moiety is one atom position farther away from the alkene, displays an encapsulation effect of 1.21 kcal mol^{-1}. Apparently, the precise position of an ether group in the substrate has a large effect on the selectivity control (Fig. 6). For the ketone and ester substrates **3f–h**, the encapsulation effects are similar to the parent
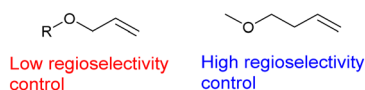
Fig. 6 Position of the ether moiety crucial for obtaining high regioselectivity control.

1-octene, **1a**. Methyl 3-butenoate **3f** is converted with a high branched selectivity with **CAT1** (l/b = 0.21). The encapsulation effect is similar to the parent substrate **1a**, showing that the high regioselectivity of **3f** is partly caused by the polarization of the alkene.

Allylbenzene derivatives

Allylbenzene derivatives are the next class of substrates that was investigated (Table 4). Allylbenzene **4a** forms a higher proportion of the branched product with the encapsulated **CAT1** and exhibits a higher encapsulation effect compared to 1-octene, **1a** (1.13 kcal mol^{-1} vs. 0.97 kcal mol^{-1}). In contrast, 3-buten-1-ylbenzene **4b** was converted with a similar regioselectivity as observed for 1-octene **1a** showing that the distal phenyl group does not affect the selectivity.

Interestingly, the presence of a methyl group on the phenyl ring, i.e. in substrates **4c–4e**, significantly changes the regioselectivity outcome with **CAT1**. A methyl group on the ortho position (**4c** (l/b = 0.32)) or the para position (**4e** (l/b = 0.27)) of the allylbenzene derivatives results in a higher branched selectivity than the parent allylbenzene **4a**. In contrast, a methyl group on the meta position, **4d**, leads to lower branched selectivity (l/b = 0.50). Control experiments with **CAT2** displayed similar regioselectivity for the allyltoluene substrates **4c–4e**, indicating that the variation in regioselectivity control is primarily caused by **CAT1**.

Since the presence of one methyl group significantly affects the regioselectivity, we also explored allylbenzene derivatives with two or three methyl groups on the phenyl ring (**4f–4i**). Analogous to the allyltoluene substrates **4c–4e**, the presence of methyl groups on the ortho and/or para positions results in high branched selectivity for **4f–4g** compared to **4a**. Two methyl groups on the meta position (**4h**) provide lower branched selectivity when converted with **CAT1** compared to **4a**. It is noteworthy that the variations in the regioselectivity are amplified with two methyl groups compared to the substrates with a single methyl group (Fig. 7).

Allylmesitylene **4i**, which has two methyl groups on the ortho positions and one methyl group on the para position, leads to an exceptionally high branched selectivity of l/b = 0.12 and displays an encapsulation effect of 1.83 kcal mol^{-1}. It is noteworthy that the branched selectivity for allylmesitylene **4i** is even higher than the branched selectivity for allylbenzene derivatives previously reported.[46]

Next, allylnaphthalene substrates **4j** and **4k** were investigated. In this class of substrates, the regioselectivity varies in the relative position of the naphthalene group with respect to the allyl reactive group. That is, **4k** is converted

Table 4 Allylbenzene, 3-buten-1-ylbenzeneallylbenzene derivatives containing 1,2 or 3 methyl groups and allylnaphthalene substrates. Conditions: [Rh(acac)(CO)$_2$] = 0.70 mmol L^{-1} in toluene, pressure (H$_2$:CO) = 20 bar, substrate/rhodium = 1000, [P($_m$Py$_3$)] = 6.4 mmol L^{-1} and 19.2 mmol l^{-1} of zinc(II) tetraphenylporphyrin for **CAT1**. No significant isomerization and/or isomerization–hydroformylation products were observed for all entries
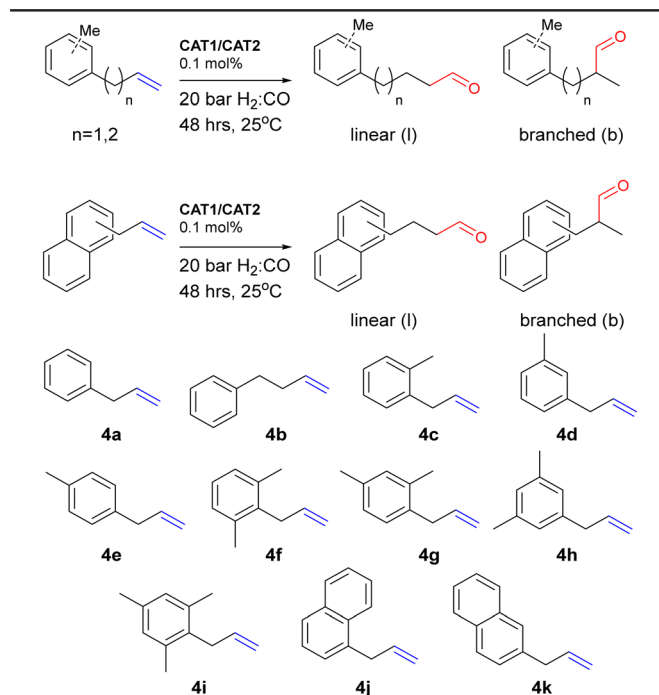
Substrate/catalyst	% conv^a	l:b^b	Encapsulation effect^c
4a/CAT1	100	0.36	1.13 kcal mol^{-1}
4a/CAT2	73	2.42	
4b/CAT1	100	0.52	1.01 kcal mol^{-1}
4b/CAT2	57	2.86	
4c/CAT1	100	0.32	1.21 kcal mol^{-1}
4c/CAT2	44	2.46	
4d/CAT1	100	0.50	1.00 kcal mol^{-1}
4d/CAT2	41	2.72	
4e/CAT1	100	0.27	1.38 kcal mol^{-1}
4e/CAT2	46	2.79	
4f/CAT1	100	0.18	1.48 kcal mol^{-1}
4f/CAT2	95	2.20	
4g/CAT1	100	0.31	1.26 kcal mol^{-1}
4g/CAT2	84	2.62	
4h/CAT1	80	0.71	0.77 kcal mol^{-1}
4h/CAT2	62	2.62	
4i/CAT1	100	0.12	1.83 kcal mol^{-1}
4i/CAT2	33	2.66	
4j/CAT1	100	0.53	0.82 kcal mol^{-1}
4j/CAT2	41	2.11	
4k/CAT1	100	0.29	1.23 kcal mol^{-1}
4k/CAT2	83	2.30	

^{a} Conversion determined by ^{1}H NMR spectroscopy. ^{b} The linear : branched ratio determined by GC. ^{c} Encapsulation calculated by subtracting the relative energy barriers of the encapsulated reaction outcome (using **CAT1**) from the unencapsulated reaction outcome (using **CAT2**).

with higher branched selectivity with **CAT1** (l/b = 0.29), whereas **4j** reacts with decreased branched selectivity (l/b = 0.53) compared to the parent allylbenzene **4a**.

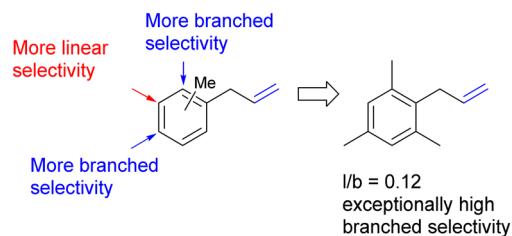This journal is © The Royal Society of Chemistry 2024

Catal. Sci. Technol., 2024, **14**, 1837–1847 | **1841**

Fig. 7 Clear regioselectivity trends for allylbenzene derivatives result in the identification of privileged allylmesitylene substrates for **CAT1**.

Next, the substrate scope was extended to allylbenzene derivatives with heteroatom substituents. We commenced our investigations with the substrates 2-allylanisole, 3-allylanisole and 4-allylanisole (**5a–5c**) (Table 5). The substrate with the methoxy moiety on the *ortho* (**5a**) or *meta* (**5b**) position is converted by **CAT1** with a significantly lower branched selectivity (l/b = 0.53 and 0.49 respectively) than that we observed for the parent allylbenzene **4a** (l/b = 0.36). In contrast, when the methoxy substituent is on the *para* position (**5c**), the branched selectivity was higher (l/b = 0.29). Again, the control experiments using **CAT2** give comparable

levels of regioselectivity for all three substrates (**5a–c**). In addition, the hydroformylation of 4-allyl-1,2-dimethoxybenzene (**5d**) and 5-allyl-1,2,3-trimethoxybenzene (**5e**), bearing two and three methoxy moieties on the phenyl ring, respectively, displays lower branched selectivity (l/b = 0.53 for **5d** and l/b = 0.53 for **5e**) than that of the parent allylbenzene **4a**.

The final subset of substrates that was explored was allylbenzene derivatives with halogen substituents (Table 6). Both 1-allyl-4-(trifluoromethyl)benzene **6a** and 1-allyl-4-fluorobenzene **6b** were converted by the caged catalyst **CAT1** with high branched selectivity (l/b = 0.15 for **6a** and l/b = 0.25 for **6b**). These results show that a substituent on the *para* position of the allylbenzene derivative results in a more branched selectivity, as improved branched selectivity is also observed for the substrates with methyl groups (**4c**) and methoxy groups (**5c**) on the *para* position with **CAT1** (*vide supra*). The allylbenzene derivative that contained a halogen atom on the *meta* position reacts with a lower regioselectivity compared to allylbenzene **4a**. In particular, 3-chloro-1-allylbenzene **6d** exhibits lower branched selectivity (l/b = 0.41), whereas the corresponding fluorine analog, 3-fluoro-1-

Table 5 Subset of allylbenzene derivatives with 1, 2 or 3 methoxy substituents on the phenyl ring. Conditions: [Rh(acac)(CO)$_2$] = 0.70 mmol L^{-1} in toluene, pressure (H$_2$:CO) = 20 bar, substrate/rhodium = 1000, [P($_m$Py$_3$)] = 6.4 mol L^{-1} and 19.2 mmol l^{-1} of zinc(II) tetraphenylporphyrin for **CAT1**
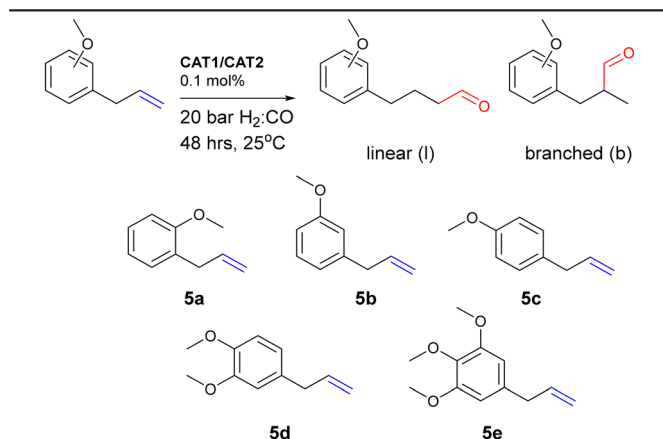
Substrate/catalyst	% conv^a	l : b^b	Encapsulation effect^c
5a/CAT1	100	0.53	0.97 kcal mol^{-1}
5a/CAT2	53	2.73	
5b/CAT1	58	0.49	0.93 kcal mol^{-1}
5b/CAT2	14	2.39	
5c/CAT1	100	0.29	1.38 kcal mol^{-1}
5c/CAT2	47	2.96	
5d/CAT1	100	0.53	0.94 kcal mol^{-1}
5d/CAT2	45	2.61	
5e/CAT1	99	0.53	0.91 kcal mol^{-1}
5e/CAT2	25	2.46	

^{a} Conversion determined by ^{1}H NMR spectroscopy. ^{b} The linear : branched ratio determined by GC. ^{c} Encapsulation calculated by subtracting the relative energy barriers of the encapsulated reaction outcome (using **CAT1**) from the unencapsulated reaction outcome (using **CAT2**).

Table 6 Allylbenzene derivatives with halogen atoms. Conditions: [Rh(acac)(CO)$_2$] = 0.70 mmol L^{-1} in toluene, pressure (H$_2$:CO) = 20 bar, substrate/rhodium = 1000, [P($_m$Py$_3$)] = 6.4 mol L^{-1} and 19.2 mmol l^{-1} of zinc(II) tetraphenylporphyrin for **CAT1**
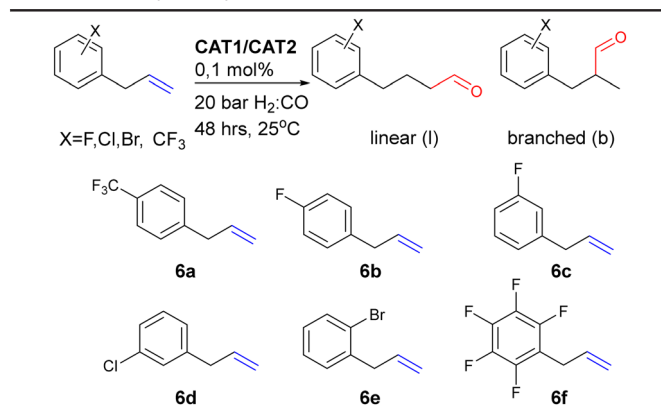
Substrate/catalyst	% conv^a	l : b^b	Encapsulation effect^c
6a/CAT1	100	0.15	1.46 kcal mol^{-1}
6a/CAT2	52	1.76	
6b/CAT1	100	0.25	1.32 kcal mol^{-1}
6b/CAT2	42	2.33	
6c/CAT1	100	0.33	1.07 kcal mol^{-1}
6c/CAT2	53	2.00	
6d/CAT1	100	0.41	0.95 kcal mol^{-1}
6d/CAT2	47	1.84	
6e/CAT1	100	0.31	1.08 kcal mol^{-1}
6e/CAT2	43	1.93	
6f/CAT1	100	0.42	0.56 kcal mol^{-1}
6f/CAT2	54	1.09	

^{a} Conversion determined by ^{1}H NMR spectroscopy. ^{b} The linear : branched ratio determined by GC. ^{c} The encapsulation effect calculated by subtracting the relative energy barriers of the encapsulated reaction outcome (using **CAT1**) from the unencapsulated reaction outcome (using **CAT2**).

allylbenzene **6c**, gives a similar encapsulation effect and regioselectivity compared to the parent allylbenzene **4a**. Substrates that have a methyl or methoxy group on this position also display a lower encapsulation effect compared to **4a** (*vide supra*).

The hydroformylation of 2-bromo-1-allylbenzene **6e** yields a similar encapsulation effect to that of allylbenzene **4a**. Allylpentafluorobenzene **6f** is converted with a branched selectivity comparable to allylbenzene **4a**. However, the control experiment with **CAT2** reveals that the C=C polarization of the substrate results in more branched product (l/b = 1.09) formation compared to that of **4a**, which is reflected in a low encapsulation effect (0.56 kcal mol^{-1}).

Optimization of reaction conditions

The exploration of the large substrate scope with **CAT1** shows a large variation in the regioselectivity control as evidenced by the large variation in encapsulation effects (0.24–1.83 kcal mol^{-1}). To shed light on this, we conducted DFT calculations (ADF, BLYP-D3, DZP) with **CAT1** and replaced one CO moiety with allylbenzene coordinated to rhodium (Fig. 8).[72–76] The lowest energy structures of the alkene coordination complex show that the phenyl ring of the substrate is in close contact (2.6 Å) with a phenyl ring of the ZnTPP building block, which is also observed in previous DFT calculations on this system.[17]

Based on the large variation in selectivity control, which cannot be explained on the basis of sterics, we propose that such interactions play a role in determining the regioisomeric outcome. Moreover, for several other hydroformylation catalyst systems, it has been established that CH–π interactions between the substrate and the catalysts play a crucial role in controlling the regioselectivity.[45,77–80]

With this in mind, we intended to optimize the regioselectivity displayed by these types of caged catalysts by using analogues of the ZnTPP building block. Previous

studies have shown that the shape of **CAT1** type cages is only preserved with ZnTPP building blocks that are functionalized with a single substituent at the *meta* position of the phenyl rings of zinc porphyrin.[17,20,81–83] When the phenyls were functionalized with two *meta* substituents and/or with a substituent on the *ortho* or *para* position, steric hindrance disrupts crucial CH–π interactions between the different ZnTTP building blocks required for the formation of the cage.[17] As a result, the branched selectivity is lost.

Hence, we used two porphyrins to generate novel catalysts; one contains an electron withdrawing substituent, CF$_3$, coined $_m$CF$_3$ZnTPP (Fig. 9, left)[84] and one contains an electron donating isopropoxide substituent (OiPr), coined $_m$-OiPrZnTPP (Fig. 9, right), on the *meta* position. Molecular modeling using DFT shows that capsules based on these building blocks ($_m$CF$_3$ZnTPP and $_m$OiPrZnTPP) provide cages **CAT3** and **CAT4**, respectively (Fig. 10) with shapes that are similar in structure to the parent **CAT1**.

CAT3 and **CAT4** were used as hydroformylation catalysts for several substrates that were evaluated in the substrate scope of **CAT1** (Table 7). We used parents 1-octene **1a** and allylbenzene **4a** and several privileged substrates that display
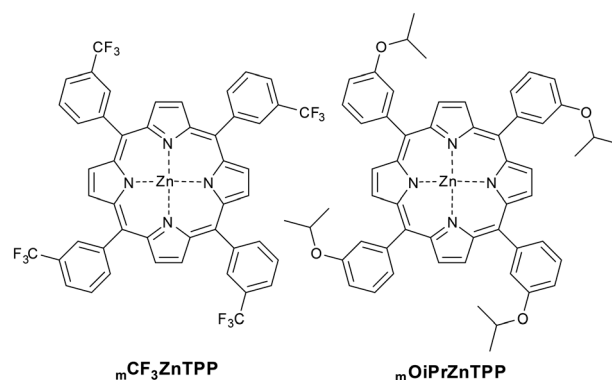
Fig. 9 ZnTPP analogs with a single substituent on the *meta* position of all phenyl rings.
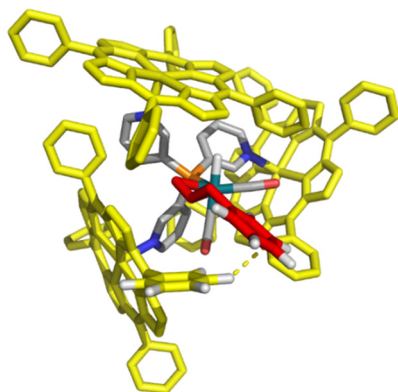
Fig. 8 DFT-optimized structure of [Rh(H)(CO)$_2$(allylbenzene)(P($_m$Py$_3$(ZnTPP)$_3$))]. The ZnTPP building block is colored yellow. The allylbenzene substrate is colored red. Hydrogens are removed for clarity apart from the relevant phenyl rings, which display CH–π interactions.
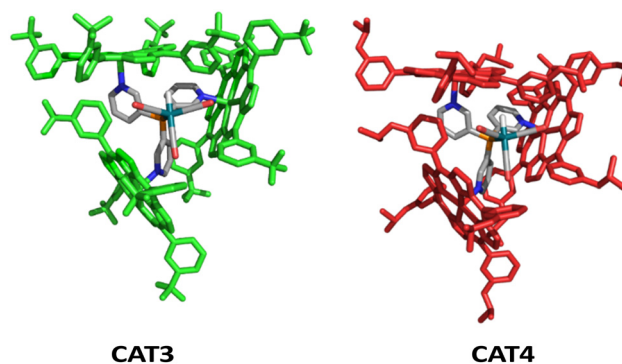
CAT3   **CAT4**

Fig. 10 DFT-optimized structures of ([Rh(H)(CO)$_3$(P($_m$Py$_3$($_m$CF$_3$ZnTPP)$_3$))]) (**CAT3**) (left) and [Rh(H)(CO)$_3$(P(($_m$Py$_3$($_m$OiPrZnTPP)$_3$))]) (**CAT4**)) (right). Porphyrin building blocks were colored green and red for clarity.

This journal is © The Royal Society of Chemistry 2024

Catal. Sci. Technol., 2024, **14**, 1837–1847 | **1843**

Table 7 Optimization of the regioselectivity by replacing the ZnTPP building block of **CAT1** with $_m$CF$_3$ZnTPP (**CAT3**) or $_m$OiPrZnTPP (**CAT4**) for a subset of substrates. Conditions: [Rh(acac)(CO)$_2$] = 0.70 mmol L^{-1} in toluene, pressure (H$_2$:CO) = 20 bar, substrate/rhodium = 1000, [P($_m$Py$_3$)] = 6.4 mol L^{-1} and 19.2 mmol l^{-1} of zinc(II) tetraphenylporphyrin for **CAT1** or analogs $_m$CF$_3$ZnTPP for **CAT3** and $_m$OiPrZnTPP for **CAT4**

Substrate/catalyst	% conv[a]	l:b[b]	Encapsulation effect[c]
1a/**CAT1**	100	0.56	0.97
1a/**CAT3**	100	0.44	1.11
1a/**CAT4**	100	0.42	1.14
4a/**CAT1**	100	0.36	1.13
4a/**CAT3**	99	0.31	1.24
4a/**CAT4**	100	0.26	1.34
1f/**CAT1**	100	0.27	1.40
1f/**CAT3**	100	0.25	1.44
1f/**CAT4**	100	0.21	1.55
2a/**CAT1**	100	0.49	1.33
2a/**CAT3**	66	0.32	1.58
2a/**CAT4**	96	0.33	1.56
3e/**CAT1**	100	0.34	1.21
3e/**CAT3**	70	0.35	1.19
3e/**CAT4**	100	0.29	1.30
4i/**CAT1**	100	0.12	**1.83**
4i/**CAT3**	100	0.19	1.56
4i/**CAT4**	100	0.11	**1.89**
6a/**CAT1**	100	0.16	1.42
6a/**CAT3**	66	0.14	1.50
6a/**CAT4**	100	0.11	1.64
6b/**CAT1**	100	0.25	1.32
6b/**CAT3**	72	0.26	1.30
6b/**CAT4**	100	0.18	1.52

[a] Conversion determined by ^{1}H NMR spectroscopy. [b] The linear : branched ratio determined by GC. [c] The encapsulation effect calculated by subtracting the relative energy barriers of the encapsulated reaction outcome (using **CAT1**, **CAT3** or **CAT4**) from the unencapsulated reaction outcome (using **CAT2**).

large encapsulation effects with **CAT1**; allylcyclohexane **1f**, vinylcyclopentane **2a**, 4-methoxybut-1-ene **3e**, allylmesitylene **4i**, 4-trifluoromethyl-1-allylbenzene **6a** and 4-fluoro-1-allylbenzene **6b**.

In general, **CAT3** and **CAT4** give high branched selectivity characteristic for the caged catalyst for all substrates investigated, which confirms that these porphyrins form cages under catalytic conditions. Importantly, the branched selectivity was higher when **CAT4** was used as the catalyst compared to the results obtained with **CAT1** for all substrates evaluated. Previous studies show that electron donating substituents at the *meta* position of the porphyrin destabilize

the cage formation due to weaker CH–π interactions between the three porpyhrins, and therefore the improved regioselectivity is not caused by stronger porphyrin assembly. More likely, this is caused by favorable noncovalent interactions between the substrate moieties and the more electron rich phenyl ring of the $_m$OiPrZnTPP building block for the branched product. For allylmesitylene **4i** and 4-trifluoromethyl-1-allylbenzene **6a**, the branched selectivity is l/b = 0.11 when **CAT4** is used as the catalyst. This is the most branched-selective hydroformylation reaction of allylbenzene derivatives known to date.[43,46,47]

In particular, the encapsulation effect of 1-octene **1a** is 0.23 kcal mol^{-1} higher for **CAT4** than for **CAT1**. Interestingly, the substrates **1a**, **2a**, **4a**, **1f** and **6a** also give a higher branched selectivity with **CAT3**, which shows that the branched selectivity of these substrates increases by using an electron withdrawing substituent or an electron donating substituent on the phenyl rings of the ZnTPP building block.

CAT3 displayed lower conversions than **CAT1** and **CAT4** for several substrates. Previous studies have shown that the presence of an electron withdrawing substituent (*i.e.* NO$_2$) on the *meta* position of the phenyl ring of the Zn porphyrin lowers the conversion compared to **CAT1** due to a lower dynamicity of the cage as a result of stronger CH–π interactions between the porphyrin building blocks of the cage.[15,17]

Conclusions

In summary, we have demonstrated that **CAT1** is able to convert a wide range of substrates with high selectivity to the branched product. Analysis of the substrate scope with **CAT1** reveals a large variation in the catalytic outcome, even when corrected for inherent substrate biases determined from the control experiments with **CAT2**. This investigation identified substrates that are converted with a high degree of selectivity enhancement to the branched product. For aliphatic substrates such as allylcyclohexane, allylcyclopentane, vinylcyclopentane, and vinylcyclohexane, large encapsulation effects are observed compared to the parent 1-octene, which shows that such cyclic shapes enhance the branched selectivity with **CAT1**. In contrast, allylether substrates display remarkably low encapsulation effects, which appear to be affected by the relative position of oxygen with respect to the alkene. Clear regioselectivity trends are also established for allylbenzene derivatives. For these substrates, substituents on the *ortho* and *para* positions improved the branched product formation and substituents on the *meta* position lowered the branched product formation compared to the unsubstituted analogue. These trends led us to identify an allylbenzene derivative allylmesitylene as a substrate that is converted by the cage catalyst **CAT1** with exceptionally high regioselectivity (l/b = 0.12).

Analysis of the substrate scope suggests that noncovalent interactions between the substrate and the walls of the encapsulated **CAT1** contribute to the regioselectivity outcome. With this in mind, we optimized these interactions using

1844 | *Catal. Sci. Technol.*, 2024, **14**, 1837–1847

This journal is © The Royal Society of Chemistry 2024

ZnTPP analogs that have a single electron donating substituent (OiPr) or electron withdrawing substituent (CF$_3$) on the *meta* position of all phenyl rings of the porphyrin as cage building blocks to generate two new encapsulated catalysts: **CAT3** and **CAT4**. Both encapsulated catalysts were able to form caged structures around the active rhodium site, and displayed the typical branched selectivity for such cages. In particular, **CAT4** gave higher branched selectivity than **CAT1** for all substrates investigated. This study shows that the exploration of a larger substrate scope with various structural elements provides new insights into how encapsulated catalysts steer the regioselectivity in the hydroformylation. Based on this insight, the cage building blocks were redesigned, leading to further improvements of the regioselectivity displayed by these encapsulated catalysts.

Author contributions

PL and JR devised the project. PL conducted the catalytic experiments, performed DFT calculations and wrote the manuscript. JR and SK supervised the project and wrote the manuscript.

Conflicts of interest

There are no conflicts to declare.

Acknowledgements

References

1 D. M. Vriezema, M. C. Aragonès, J. A. A. W. Elemans, J. J. L. M. Cornelissen, A. E. Rowan and R. J. M. Nolte, *Chem. Rev.*, 2005, **105**, 1445–1489.

2 S. H. A. M. Leenders, R. Gramage-Doria, B. De Bruin and J. N. H. Reek, *Chem. Soc. Rev.*, 2015, **44**, 433–448.

3 M. Raynal, P. Ballester, A. Vidal-Ferran and P. W. N. M. van Leeuwen, *Chem. Soc. Rev.*, 2014, **43**, 1660–1733.

4 M. Raynal, P. Ballester, A. Vidal-Ferran and P. W. N. M. van Leeuwen, *Chem. Soc. Rev.*, 2014, **43**, 1734–1787.

5 M. J. Wiester, P. A. Ulmann and C. A. Mirkin, *Angew. Chem., Int. Ed.*, 2011, **50**, 114–137.

6 L. Catti, Q. Zhang and K. Tiefenbacher, *Chem. – Eur. J.*, 2016, **22**, 9060–9066.

7 C. J. Brown, F. D. Toste, R. G. Bergman and K. N. Raymond, *Chem. Rev.*, 2015, **115**, 3012–3035.

8 R. J. Severinsen, G. J. Rowlands and P. G. Plieger, *J. Inclusion Phenom. Macrocyclic Chem.*, 2019, **96**, 29–42.

9 M. Morimoto, S. M. Bierschenk, K. T. Xia, R. G. Bergman, K. N. Raymond and F. D. Toste, *Nat. Catal.*, 2020, **3**, 969–984.

10 J. Meeuwissen and J. N. H. Reek, *Nat. Chem.*, 2010, **2**, 615–621.

11 T. Gadzikwa, R. Bellini, H. L. Dekker and J. N. H. Reek, *J. Am. Chem. Soc.*, 2012, **134**, 2860–2863.

12 C. García-Simón, R. Gramage-Doria, S. Raoufmoghaddam, T. Parella, M. Costas, X. Ribas and J. N. H. Reek, *J. Am. Chem. Soc.*, 2015, **137**, 2680–2687.

13 S. S. Nurttila, W. Brenner, J. Mosquera, K. M. van Vliet, J. R. Nitschke and J. N. H. Reek, *Chem. – Eur. J.*, 2019, **25**, 609–620.

14 V. F. Slagt, J. N. H. Reek, P. C. J. Kamer and P. W. N. M. Van Leeuwen, *Angew. Chem., Int. Ed.*, 2001, **40**, 4271–4274.

15 V. F. Slagt, P. C. J. Kamer, P. W. N. M. Van Leeuwen and J. N. H. Reek, *J. Am. Chem. Soc.*, 2004, **126**, 1526–1536.

16 M. Kuil, T. Soltner, P. W. N. M. Van Leeuwen and J. N. H. Reek, *J. Am. Chem. Soc.*, 2006, **128**, 11344–11345.

17 V. Bocokić, A. Kalkan, M. Lutz, A. L. Spek, D. T. Gryko and J. N. H. Reek, *Nat. Commun.*, 2013, **4**, 2670.

18 M. Jouffroy, R. Gramage-Doria, D. Armspach, D. Sémeril, W. Oberhauser, D. Matt and L. Toupet, *Angew. Chem., Int. Ed.*, 2014, **53**, 3937–3940.

19 X. Wang, S. S. Nurttila, W. I. Dzik, R. Becker, J. Rodgers and J. N. H. Reek, *Chem. – Eur. J.*, 2017, **23**, 14769–14777.

20 L. J. Jongkind and J. N. H. Reek, *Chem. – Asian J.*, 2020, **15**, 867–875.

21 C. Gibson and J. Rebek, *Org. Lett.*, 2002, **4**, 1887–1890.

22 D. H. Leung, R. G. Bergman and K. N. Raymond, *J. Am. Chem. Soc.*, 2007, **129**, 2746–2747.

23 D. H. Leung, R. G. Bergman and K. N. Raymond, *J. Am. Chem. Soc.*, 2006, **128**, 9781–9797.

24 T. A. Bender, R. G. Bergman, K. N. Raymond and F. D. Toste, *J. Am. Chem. Soc.*, 2019, **141**, 11806–11810.

25 M. Otte, P. F. Kuijpers, O. Troeppner, I. Ivanovič-Burmazovič, J. N. H. Reek and B. De Bruin, *Chem. – Eur. J.*, 2014, **20**, 4880–4884.

26 M. Otte, P. F. Kuijpers, O. Troeppner, I. Ivanovič-Burmazovič, J. N. H. Reek and B. De Bruin, *Chem. – Eur. J.*, 2013, **19**, 10170–10178.

27 P. F. Kuijpers, M. Otte, M. Dürr, I. Ivanović-Burmazović, J. N. H. Reek and B. De Bruin, *ACS Catal.*, 2016, **6**, 3106–3112.

28 M. L. Merlau, M. D. P. Mejia, S. T. Nguyen and J. T. Hupp, *Angew. Chem., Int. Ed.*, 2001, **40**, 4239–4242.

29 J. L. Suk, S. H. Cho, K. L. Mulfort, D. M. Tiede, J. T. Hupp and S. B. T. Nguyen, *J. Am. Chem. Soc.*, 2008, **130**, 16828–16829.

30 P. Zhang, J. Meijide Suárez, T. Driant, E. Derat, Y. Zhang, M. Ménand, S. Roland and M. Sollogoub, *Angew. Chem., Int. Ed.*, 2017, **56**, 10821–10825.

31 R. Gramage-Doria, J. Hessels, S. H. A. M. Leenders, O. Tröppner, M. Dürr, I. Ivanović-Burmazović and J. N. H. Reek, *Angew. Chem., Int. Ed.*, 2014, **53**, 13380–13384.

32 Q.-Q. Wang, S. Gonell, S. H. a. M. Leenders, M. Dürr, I. Ivanović-Burmazović and J. N. H. Reek, *Nat. Chem.*, 2016, **8**, 225–230.

This journal is © The Royal Society of Chemistry 2024

Catal. Sci. Technol., 2024, **14**, 1837–1847 | 1845

33 M. Guitet, P. Zhang, F. Marcelo, C. Tugny, J. Jiménez-Barbero, O. Buriez, C. Amatore, V. Mouriès-Mansuy, J.-P. Goddard, L. Fensterbank, Y. Zhang, S. Roland, M. Ménand and M. Sollogoub, *Angew. Chem., Int. Ed.*, 2013, **52**, 7213–7218.

34 A. W. Kleij and J. N. H. Reek, *Chem. – Eur. J.*, 2006, **12**, 4218–4227.

35 L. J. Jongkind, X. Caumes, A. P. T. Hartendorp and J. N. H. Reek, *Acc. Chem. Res.*, 2018, **51**, 2115–2128.

36 S. Das, G. W. Brudvig and R. H. Crabtree, *Chem. Commun.*, 2008, 413–424.

37 R. Franke, D. Selent and A. Börner, *Chem. Rev.*, 2012, **112**, 5675–5732.

38 S. S. Nurttila, P. R. Linnebank, T. Krachko and J. N. H. Reek, *ACS Catal.*, 2018, **8**, 3469–3488.

39 P. W. N. M. van Leeuwen, *Homogeneous Catalysis: Understanding the art*, Springer Netherlands, Dordrecht, 2004, vol. 1.

40 P. W. N. M. van Leeuwen, C. P. Casey and G. T. Whiteker, *Rhodium catalyzed hydroformylation*, Kluwer Academic Publishers, Dordrecht, 2000.

41 M. Kranenburg, Y. E. M. van der Burgt, P. C. J. Kamer, P. W. N. M. van Leeuwen, K. Goubitz and J. Fraanje, *Organometallics*, 1995, **14**, 3081–3089.

42 C. P. Casey, G. T. Whiteker, M. G. Melville, L. M. Petrovich, J. A. Gavney and D. R. Powell, *J. Am. Chem. Soc.*, 1992, **114**, 5535–5543.

43 A. Phanopoulos and K. Nozaki, *ACS Catal.*, 2018, **8**, 5799–5809.

44 G. M. Noonan, J. A. Fuentes, C. J. Cobley and M. L. Clarke, *Angew. Chem., Int. Ed.*, 2012, **51**, 2477–2480.

45 P. Dingwall, J. A. Fuentes, L. Crawford, A. M. Z. Slawin, M. Bühl and M. L. Clarke, *J. Am. Chem. Soc.*, 2017, **139**, 15921–15932.

46 L. Iu, J. A. Fuentes, M. E. Janka, K. J. Fontenot and M. L. Clarke, *Angew. Chem., Int. Ed.*, 2019, **58**, 2120–2124.

47 Z. Yu, M. S. Eno, A. H. Annis and J. P. Morken, *Org. Lett.*, 2015, **17**, 3264–3267.

48 M. Y. S. Ibrahim, J. A. Bennett, D. Mason, J. Rodgers and M. Abolhasani, *J. Catal.*, 2022, **409**, 105–117.

49 L. A. Van Der Veen, P. C. J. Kamer and P. W. N. M. Van Leeuwen, *Angew. Chem., Int. Ed.*, 1999, **38**, 336–338.

50 D. Selent, K. D. Wiese, D. Röttger and A. Börner, *Angew. Chem., Int. Ed.*, 2000, **39**, 1639–1641.

51 T. E. Lightburn, M. T. Dombrowski and K. L. Tan, *J. Am. Chem. Soc.*, 2008, **130**, 9210–9211.

52 C. L. Joe, T. P. Blaisdell, A. F. Geoghan and K. L. Tan, *J. Am. Chem. Soc.*, 2014, **136**, 8556–8559.

53 C. U. Grünanger and B. Breit, *Angew. Chem., Int. Ed.*, 2008, **120**, 7456–7459.

54 C. U. Grünanger and B. Breit, *Angew. Chem., Int. Ed.*, 2010, **49**, 967–970.

55 T. Šmejkal and B. Breit, *Angew. Chem., Int. Ed.*, 2008, **47**, 311–315.

56 T. Šmejkal, D. Gribkov, J. Geier, M. Keller and B. Breit, *Chem. – Eur. J.*, 2010, **16**, 2470–2478.

57 W. Fang, F. Bauer, Y. Dong and B. Breit, *Nat. Commun.*, 2019, **10**, 1–9.

58 W. Fang and B. Breit, *Angew. Chem., Int. Ed.*, 2018, **57**, 14817–14821.

59 P. R. Linnebank, S. F. Ferreira, A. M. Kluwer and J. N. H. Reek, *Chem. – Eur. J.*, 2020, **26**, 8214–8219.

60 J. N. H. Reek, B. de Bruin, S. Pullen, T. J. Mooibroek, A. M. Kluwer and X. Caumes, *Chem. Rev.*, 2022, **122**, 12308–12369.

61 M. Sigrist, Y. Zhang, C. Antheaume and P. Dydio, *Angew. Chem., Int. Ed.*, 2022, **61**, e202116406.

62 With the selection of **CAT2** as the model system for the caged catalysts, we have a reference system in which all the experimental details are the same, with the exception of the presence of the specified porphyrin. The generation of monoligated complexes, similar to **CAT1**, is only possible with ligands that differ largely in electronic and steric properties. Such variation in ligand properties does not allow for a direct comparison where cage formation is the sole variable under study. These factors will significantly complicate the analysis by introducing multiple variables that affect the catalytic outcome. In contrast, the use of **CAT2** offers a more controlled and consistent framework, where the effects of porphyrin addition can be isolated and evaluated, and interpretation is supported by previous results and theoretical calculations.

63 P. R. Linnebank, D. A. Poole, A. M. Kluwer and J. N. H. Reek, *Faraday Discuss.*, 2023, **244**, 169–185.

64 I. Jacobs, B. De Bruin and J. N. H. Reek, *ChemCatChem*, 2015, **7**, 1708–1718.

65 P. C. J. Kamer, A. Van Rooy, G. C. Schoemaker and P. W. N. M. Van Leeuwen, *Coord. Chem. Rev.*, 2004, **248**, 2409–2424.

66 S. C. Van der Slot, P. C. J. Kamer, P. W. N. M. Van Leeuwen, J. A. Iggo and B. T. Heaton, *Organometallics*, 2001, **20**, 430–441.

67 A. Van Rooy, J. N. H. De Bruijn, K. F. Roobeek, P. C. J. Kamer and P. W. N. M. Van Leeuwen, *J. Organomet. Chem.*, 1996, **507**, 69–72.

68 L. Diab, T. Šmejkal, J. Geier and B. Breit, *Angew. Chem., Int. Ed.*, 2009, **48**, 8022–8026.

69 I. Piras, R. Jennerjahn, R. Jackstell, A. Spannenberg, R. Franke and M. Beller, *Angew. Chem., Int. Ed.*, 2011, **50**, 280–284.

70 R. I. McDonald, G. W. Wong, R. P. Neupane, S. S. Stahl and C. R. Landis, *J. Am. Chem. Soc.*, 2010, **132**, 14027–14029.

71 N. Ruiz, A. Polo, S. Castillón and C. Claver, *J. Mol. Catal. A: Chem.*, 1999, **137**, 93–100.

72 C. F. Guerra, J. G. Snijders, G. Velde and E. J. Baerends, *Theor. Chem. Acc.*, 1998, 391–403.

73 E. J. Baerends, T. Ziegler, J. Autschbach, D. Bashford, A. Bérces, F. M. Bickelhaupt, C. Bo, P. M. Boerrigter, L. Cavallo, D. P. Chong, L. Deng, R. M. Dickson, D. E. Ellis, M. van Faassen, L. Fan, T. H. Fischer, C. F. Guerra and M. Franchini, ADF2017, SCM, Theoretical Chemistry, Vrije Universiteit, Amsterdam, The Netherlands, 2017.

1846 | *Catal. Sci. Technol.*, 2024, **14**, 1837–1847

This journal is © The Royal Society of Chemistry 2024

74 A. D. Becke, *Phys. Rev. A*, 1988, **38**, 3098–3100.

75 C. Lee, W. Yang and R. G. Parr, *Phys. Rev. B*, 1988, **37**, 785–789.

76 E. van Lenthe, A. Ehlers and E. Baerends, *J. Chem. Phys.*, 1999, **110**, 8943–8953.

77 M. Kumar, R. V. Chaudhari, B. Subramaniam and T. A. Jackson, *Organometallics*, 2014, **33**, 4183–4191.

78 Y. Dangat, S. Popli and R. B. Sunoj, *J. Am. Chem. Soc.*, 2020, **142**, 17079–17092.

79 M. Kumar, R. V. Chaudhari, B. Subramaniam and T. A. Jackson, *Organometallics*, 2014, **33**, 4183–4191.

80 H. J. Davis and R. J. Phipps, *Chem. Sci.*, 2017, **8**, 864–877.

81 A. W. Kleij, M. Kuil, D. M. Tooke, A. L. Spek and J. N. H. Reek, *Inorg. Chem.*, 2005, **44**, 7696–7698.

82 A. W. Kleij, M. Lutz, A. L. Spek, P. W. N. M. Van Leeuwen and J. N. H. Reek, *Chem. Commun.*, 2005, 3661–3663.

83 M. Kuil, P. E. Goudriaan, A. W. Kleij, D. M. Tooke, A. L. Spek, P. W. N. M. Van Leeuwen and J. N. H. Reek, *Dalton Trans.*, 2007, 2311–2320.

84 R. Bellini and J. N. H. Reek, *Chem. – Eur. J.*, 2012, **18**, 13510–13519.

This journal is © The Royal Society of Chemistry 2024

Catal. Sci. Technol., 2024, **14**, 1837–1847 | 1847